RSC Advances

PAPER

View Article Online
View Journal | View Issue

Cite this: *RSC Adv.*, 2019, **9**, 36334

A uniform few-layered carbon coating derived from self-assembled carboxylate monolayers capable of promoting the rate properties and durability of commercial TiO_2†

Meng Huang,[a] Hui-Ling Zhu,[b] Yong-Xin Qi,[a] Ning Lun*[a] and Yu-Jun Bai *[a]

The poor cyclability and rate property of commercial TiO_2 (c-TiO_2) hinder its utilization in lithium-ion batteries (LIBs). Coating carbon is one of the ways to ameliorate the electrochemical performance. However, how to effectively form a uniform thin carbon coating is still a challenge. On the basis of the strong interaction of the TiO_2 surface with carboxyl groups, herein a new tactic to achieve uniform and thin carbon layers on the c-TiO_2 particles was proposed. When mixing c-TiO_2 with citric acid containing carboxyl groups in deionized water, the high-affinity adsorption of TiO_2 for carboxyl groups resulted in self-assembled carboxylate monolayers on the surface of TiO_2 which evolved into a uniform few-layered amorphous carbon coating during carbonizing at 750 °C. The product derived from the mixture of c-TiO_2 and citric acid with a mass ratio of 1 : 0.3 exhibits the optimal performance, revealing a high specific capacity (256.6 mA h g^{-1} after 50 cycles at 0.1 A g^{-1}) and outstanding cycling stability (retaining a capacity of 160.0 mA h g^{-1} after 1000 cycles at 0.5 A g^{-1}). The greatly enhanced capacity and cyclability correlate with the uniform few-layered carbon coating which not only ameliorates the electronic conductivity of c-TiO_2 but also avoids the reduction in ionic conductivity caused by thick carbon layers and redundant carbon.

Received 8th October 2019
Accepted 4th November 2019

DOI: 10.1039/c9ra08141k

rsc.li/rsc-advances

1. Introduction

The rapid development of electric vehicles, hybrid electric vehicles and large-scale renewable energy storage equipment has prompted the urgent need for low-cost and environmentally friendly energy storage systems. Li-ion batteries (LIBs) have gained great success recently in commerce on account of their high energy and power densities, good stability and safety.[1,2] However, the electrode materials still face some intractable obstacles, mainly including low electronic and/or ionic conductivities, and unavoidable capacity decay during charging and discharging.

Insertion-type anodes, especially Ti-based oxides, exhibit high safety. TiO_2 has a series of advantages, such as environmental benignity, abundance in the earth, low price, high chemical stability, low volume change (<4%) and small structural strain in lithiation/delithiation process.[3,4] Nevertheless, the low electronic conductivity and poor Li-ion conductivity are the main factors restricting its application in LIBs.[5,6] To date, extensive explorations have been carried out to solve these issues by ion-doping,[7] scaling down the particle size to nanometer for shortening Li-ion diffusion length,[8,9] appropriately controlling to form novel morphology,[10–12] and coating with conductive carbon materials,[13–15] among which the last one is commonly simple and efficient to improve the electrochemical performance of TiO_2. However, the TiO_2 employed in the available investigations was mostly prepared by the precursors with high cost, regardless of the economy for applications.

Commercially available anatase TiO_2 with low cost is conveniently fabricated by acid etching titanium ore. However the impurities in the commercial TiO_2 (c-TiO_2) have serious effect on the electrochemical performance,[16] only several reports are concerning with the electrochemical performance of c-TiO_2. Sulfate radicals are the dominant impurities in c-TiO_2, which could be eliminated by heating the c-TiO_2 above 750 °C. Furthermore, coating carbon at 750 °C with the carbon source of glucose could not only effectively remove the sulfate radicals but also greatly meliorate the electrochemical properties of c-TiO_2, achieving a capacity of 203.4 mA h g^{-1} after 250 cycles at 0.5 A g^{-1}.[17] When the c-TiO_2 was coated with soft carbon derived from pitch, a capacity of 140.2 mA h g^{-1} was retained after 1000 cycles at 0.5 A g^{-1}.[18] Thus the c-TiO_2 composited with carbon at

[a]*Key Laboratory for Liquid–Solid Structural Evolution and Processing of Materials (Ministry of Education), Shandong University, Jinan 250061, PR China. E-mail: byj97@sdu.edu.cn; lunning66@sdu.edu.cn; Fax: +86 531 88392315; Tel: +86 531 88392315*

[b]*School of Materials Science and Engineering, Shandong University of Science and Technology, Qingdao, 266590, PR China*

† Electronic supplementary information (ESI) available. See DOI: 10.1039/c9ra08141k

temperatures above 750 °C could denote elevated specific capacities owing to the removal of the sulfate radicals and the improvement in electrical conductivity, but the cyclability is still unsatisfactory, possibly because of the difficulty in tailoring the uniform formation of the carbon coating around the TiO_2 particles. The incomplete carbon coating could not isolate TiO_2 from electrolyte, and the electronic conductivity could not be thoroughly revealed. Moreover, superfluous carbon also affects the rate performance and cycling stability of TiO_2 on account of the poor performance of carbon materials at high current rate.

Due to the low volume variation during the lithiation/delithiation in TiO_2, the optimum carbon content is to form the uniform and thin coating as soon as possible, not only enhancing the electric conductivity but also facilitating Li-ion migration. How to effectively achieve the homogenous thin carbon coating is still a challenge.

According to a very recent report,[19] TiO_2 could selectively absorb carboxylic acid due to the high-affinity adsorption resulted from the bidentate binding, leading to self-assembled carboxylate monolayers on the surface of TiO_2. This strong adsorption phenomenon might find other applications besides self-cleaning and photocatalysis. In this work, citric acid (CA) with carboxyl groups was chosen as the carbon source to manufacture the carbon-coated c-TiO_2 at 750 °C, aiming at to obtain uniform and thin carbon coating layers for optimizing the electrochemical performance of c-TiO_2. As expected, the rate performance and cycling stability were significantly raised by simply adjusting the mass ratio of CA/TiO_2, achieving a high specific capacity of 256.6 mA h g^{-1} at 0.1 A g^{-1} and 168.2 mA h g^{-1} at 0.5 A g^{-1} even after 1000 cycles. The mechanism involved was discussed by virtue of several characterization methods.

2. Experimental

2.1. Fabrication of TiO_2/C

The c-TiO_2 (purity of 99.19 wt%, 0.5 wt% SO_4^{2-}, specific surface area of 350 m^2 g^{-1}) was purchased from Panzhihua TaiDu Chemical Industry Co. Ltd, identical to that in our previous work.

The carbon-coated c-TiO_2 was fabricated by two simple steps. (1) CA of 0.6, 0.9 and 1.2 g was dissolved in 50 mL deionized water separately, then 3.0 g c-TiO_2 was added into each solution and magnetically stirred for 30 min in a crucible (*i.e.* the mass ratio for CA/c-TiO_2 is 0.2, 0.3 and 0.4 one by one), the uniform mixtures were dried in an oven at 105 °C for 12 h to obtain the precursors. (2) The dried precursors were calcined in a horizontal tube furnace at 750 °C for 5 h (at a heating rate of 5 °C min^{-1}) under N_2 atmosphere. The calcination products were consecutively labeled as TiO_2/C-20, TiO_2/C-30 and TiO_2/C-40 in terms of the mass percent of CA/c-TiO_2.

2.2. Characterization

Crystal structure was identified by powder X-ray diffraction (XRD) in a Rigaku Dmax-2500 diffractometer with Cu Kα radiation in 2θ range from 10 to 90°. Raman spectra (Lab-RAM HR800 Raman spectroscope) were adopted to characterize carbon material using argon ion laser excitation with wavelength of 632.81 nm. High-resolution transmission electron microscopy (HRTEM, JEOL JEM-2100 microscope) was employed to analyze microstructure. Carbon content was determined by thermogravimetric analysis (TGA) *via* heating the carbon-coated samples in air to 700 °C in a TGA/DSC1/1600 apparatus.

2.3. Electrode preparation and performance test

The electrochemical properties of TiO_2/C were tested by assembling coin-type half cells (CR 2025) in a glove box filled with Ar atmosphere. The active substance, acetylene black and polyvinylidene difluoride were mixed according to a mass ratio of 8 : 1 : 1 in solvent of *n*-methyl pyrrolidinone. The homogeneous mixture was coated on Cu foil followed by vacuum drying for 12 h at 120 °C. The other cell components include counter electrode of Li foil, separator of Celgard 2300, electrolyte containing 1 M $LiPF_6$ dissolved in ethyl carbonate and dimethyl carbonate with a volume ratio of 1 : 1.

Land CT2001A battery test systems were employed to evaluate the electrochemical performance in a potential range of 0.02–3.0 V (*vs.* Li/Li^+) at 25 °C. An IviumStat electrochemical workstation was adopted to test cyclic voltammogram (CV) between 0.02 and 3.0 V at a scanning rate of 0.3 mV s^{-1} and electrochemical impedance spectra (EIS) in a frequency range of 10^{-2}–10^5 Hz with a signal amplitude of 3 mV.

3. Results and discussion

3.1. TG/DTG curves and FTIR spectra for determining the interaction between TiO_2 and CA

In order to determine the interaction between TiO_2 and CA, TG/DTG curves were measured in N_2 atmosphere for the pristine CA and the precursor of TiO_2/C-30. For CA, the dominant weight loss around 200 °C is followed by a slight weight loss around 250 °C owing to the pyrolysis of CA (Fig. 1a), and the intensity ratio for the latter DTG peak to the former one is 0.072. However, for the precursor of TiO_2/C-30, besides the weight loss around 200 °C, another weight loss happened around 375 °C (Fig. 1b), and the intensity ratio for the two DTG peaks is 0.2569. Apparently, the weight loss at the second stage for the TiO_2/C-30 precursor shifts to higher temperature, and the ratio is much high than that for CA, demonstration the strong interaction between TiO_2 and CA due to the high-affinity adsorption of TiO_2 surface for carboxyl groups, as reported in the literature.[19] The self-assembled carboxylate monolayers on the surface of TiO_2 facilitates to evolved into uniform few-layered carbon coating during subsequent carbonization at 750 °C.

The interaction between TiO_2 and CA was also confirmed by FTIR (Fig. 1c). In the spectra of TiO_2/C-30 precursor and c-TiO_2, the broad peak around 400–900 cm^{-1} originates from the Ti–O bond of TiO_2,[20] the adsorption peaks near 1200 and 1400 cm^{-1} from the –OH in citric acid, the peak around 1634 cm^{-1} from the surface hydroxyl group, and the adsorption bands in the region of 3000–3500 cm^{-1} from the vibration of the adsorbed

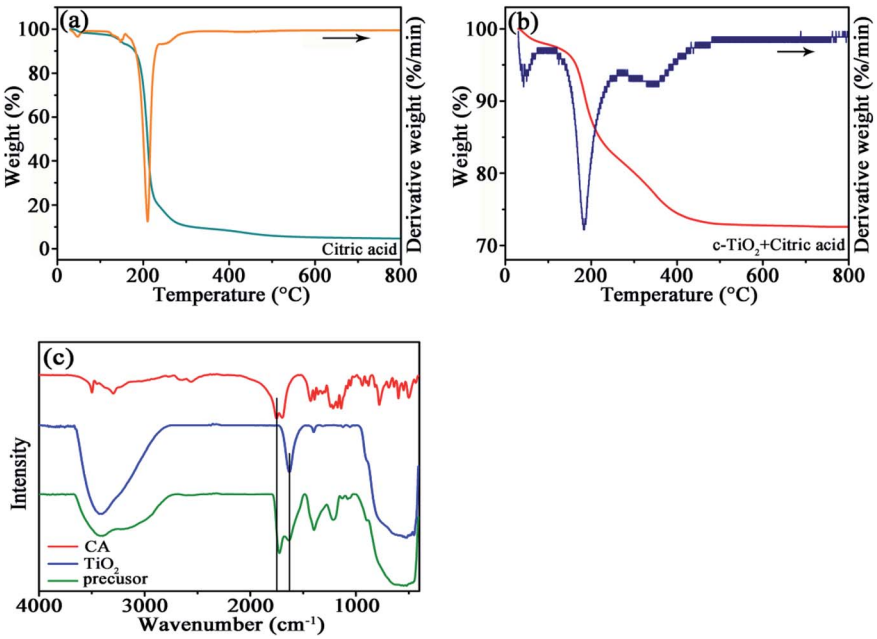

Fig. 1 TG/DTG curves of CA (a), TiO_2/C-30 precursor (b) at the heating rate of 10 °C min^{-1} under N_2 atmosphere, and (c) FTIR spectra of CA, TiO_2 and TiO_2/C-30 precursor.

water.[21] The absorption band at 1751 cm^{-1} in CA is related to the C=O from carboxyl groups.[22,23] No deviation occurs for the adsorption peak of surface hydroxyl group at 1634 cm^{-1}, whereas the position of C=O bond in TiO_2/C-30 precursor shifts to 1724 cm^{-1}, denoting the strong interaction between TiO_2 and carboxyl group as observed in the TG/DTG curves.

3.2. Structure and carbon content evaluation

The XRD patterns (Fig. 2a) of TiO_2, TiO_2/C-20, TiO_2/C-30, and TiO_2/C-40 calcined at 750 °C manifest similar diffractions to anatase TiO_2 (JCPDS no. 71-1166). The peaks of bare TiO_2 are narrower and stronger than those of TiO_2/C, demonstrating the

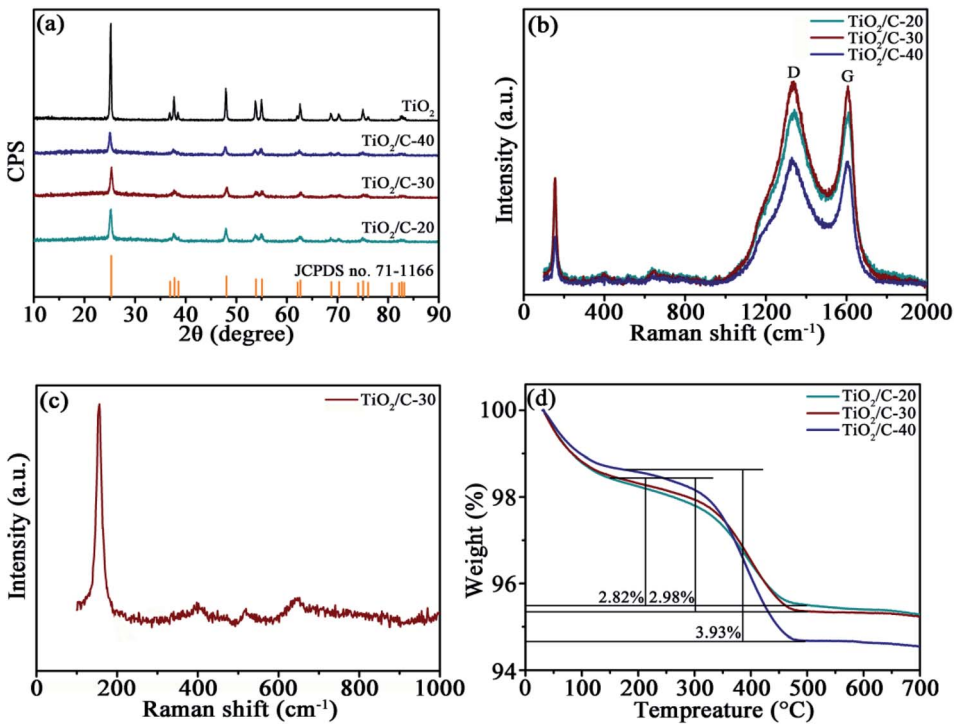

Fig. 2 (a) XRD patterns of TiO_2 and TiO_2/C, (b) Raman spectra of TiO_2/C, (c) partially enlarged Raman spectrum TiO_2/C-30, and (d) TG curves of TiO_2/C.

grain growth of TiO_2 in the absence of carbon layer. Calculated by the Scherrer equation $D = K\lambda/(\beta \cos \theta)$, the average crystallite sizes are 38.7 nm for TiO_2, 14.7 nm for TiO_2/C-20, 13.9 nm for TiO_2/C-30 and 10.1 nm for TiO_2/C-40 in terms of the (101) plane, further confirming the hindered growth of TiO_2 crystallites in the presence of carbon derived from CA. No distinct carbon diffractions could be identified due to the low content and amorphous structure, as evidenced by Raman spectra and TG analysis.

The presence of carbon in TiO_2/C was corroborated by Raman spectra (Fig. 2b). The characteristic D (around 1341 cm^{-1}) and G bands (around 1606 cm^{-1}) represent amorphous and graphitized carbon, respectively. The relative intensity ratio (I_D/I_G) of the two bands is 1.016 for TiO_2/C-20, 1.024 for TiO_2/C-30 and 1.011 for TiO_2/C-40, manifesting the low graphitization degree of the CA-derived carbon. The partially enlarged Raman spectrum between 100–1000 cm^{-1} for TiO_2/C-30 (Fig. 2c) indicates the characteristic peaks at 154, 397, 521 and 631 cm^{-1} resulted from anatase TiO_2.[24,25]

The carbon content was assessed by TGA at the heating rate of 10 °C min^{-1} under air atmosphere (Fig. 2d). The curves contain two weight loss stages; the one below 200 °C is attributed to the elimination of moisture absorbed on the samples, and the other one between 200 and 500 °C results from the combustion of carbon. Consequently, the carbon content is 2.82 wt% for TiO_2/C-20, 2.98 wt% for TiO_2/C-30, and 3.93 wt% for TiO_2/C-40.

3.3. Microstructure examination

The interaction of carbon with TiO_2 was examined by TEM (Fig. 3). Homogeneous microstructure could be observed from the low magnification images (Fig. 3a, c and e). The high-resolution images (Fig. 3b, d and f) illustrate the interplanar spacing of 0.35 nm which is consistent with that of the (101)

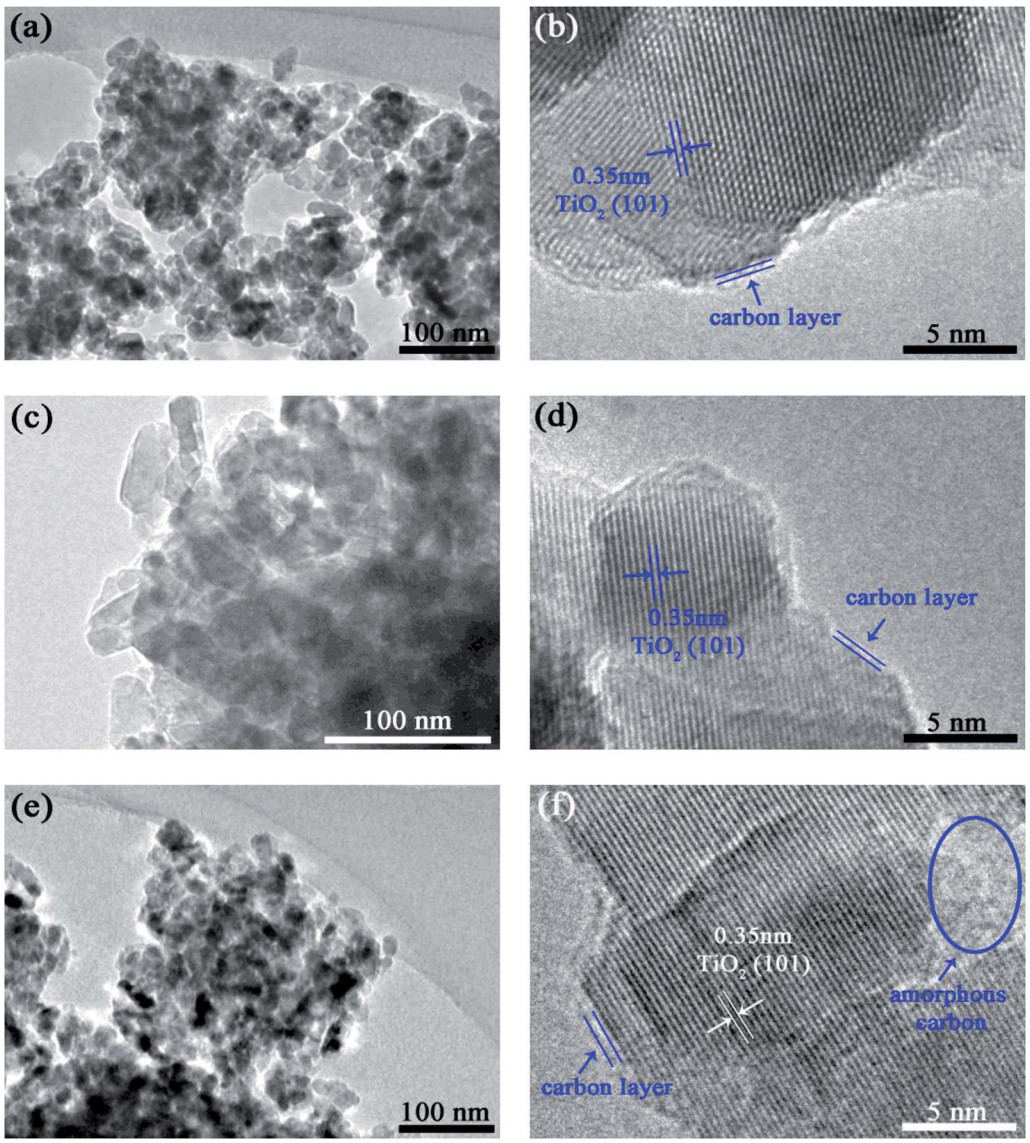

Fig. 3 TEM images of TiO_2/C-20 (a and b), TiO_2/C-30 (c and d), TiO_2/C-40 (e and f).

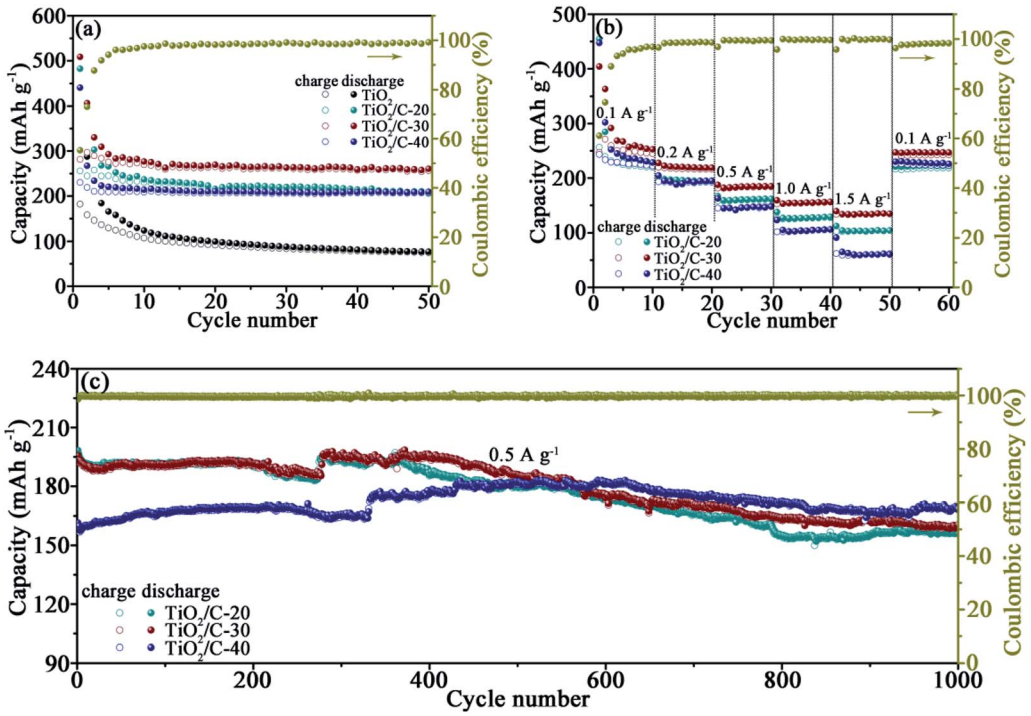

Fig. 4 (a) Cycling performance of TiO_2 and TiO_2/C at 0.1 A g^{-1}, (b) rate performance of TiO_2/C, (c) cycling performance of TiO_2/C at 0.5 A g^{-1}.

plane of anatase TiO_2. Carbon coating about 2–3 carbon layers in thickness is discernible on the surface of TiO_2 particles. The coating for TiO_2/C-30 is uniform (Fig. 3d), yet is discontinuous for TiO_2/C-20 because the carbon content is too low to fully cover the TiO_2 particles (Fig. 3b), while for TiO_2/C-40, besides the unintermitted few-layered carbon, some amorphous carbon presents among the particles owing to the higher carbon content (Fig. 3f). The uniform and thin carbon coating could facilitate electron transfer, compensating for the poor electronic conductivity of c-TiO_2. In addition, the carbon layer is also conducive to maintaining the stability of the structure,[26] thus the structure will not easy to be destroyed during the Li^+ shuttle, which is beneficial to improving the electrochemical performance of c-TiO_2.

3.4. Electrochemical performance assessment

The electrochemical performance of TiO_2/C was firstly assessed by galvanostatically discharging/charging at 0.1 A g^{-1} with the active substance of about 1.7–2.3 mg cm^{-2} on each electrode (Fig. 4a). The initial coulombic efficiencies (CE) are 26.2%, 53.0%, 55.3% and 52.2% for TiO_2, TiO_2/C-20, TiO_2/C-30 and TiO_2/C-40, respectively, indicative of the enhanced CE after coating carbon derived from CA. The formation of SEI films in the 1st cycle is responsible for the low CE. Except for the initial cycles, the CE is almost close to 100%, conducive to maintaining good cycling stability. After the initial several cycles, the capacities of the products tend to be stable, achieving lithiation capacities of 74.9, 205.7, 256.6 and 206.8 mA h g^{-1} after the 50th cycle for TiO_2, TiO_2/C-20, TiO_2/C-30 and TiO_2/C-40, respectively. The capacity of TiO_2/C is evidently higher than that of the bare TiO_2, because the thin carbon coating could separate the TiO_2 particles from electrolyte, preventing some side reactions and thus meliorating the electrochemical performance of c-TiO_2.

To understand the structural stability with cycling, the XRD patterns of TiO_2/C-30 were acquired before cycling and after 100 charge/discharge cycles at 0.1 A g^{-1} (Fig. S1†). Apparently, the structure after 100 cycles is identical to that prior to cycling with the Cu diffractions as a reference.

Rate capabilities were tested at 0.1, 0.2, 0.5, 1.0, 1.5 and 0.1 A g^{-1} for every 10 cycles (Fig. 4b), the average capacity at each current density and the capacity retention relative to the capacity at the initial 0.1 A g^{-1} are summarized in Table 1 for

Table 1 Average lithiation capacities (mA h g^{-1}) and capacity retention (%) at diverse current densities (A g^{-1})

	Capacities/capacity retention at varied current densities					
Samples	0.1	0.2	0.5	1.0	1.5	0.1
TiO_2/C-20	221.3/100	193.1/87.3	160.4/72.5	127.2/57.5	102.8/46.5	218.7/98.8
TiO_2/C-30	245.8/100	216.6/88.1	183.3/74.6	154.4/62.8	133.7/54.4	242.6/98.7
TiO_2/C-40	224.8/100	191.1/85.0	147.5/65.6	105.3/46.8	60.4/26.9	224.1/99.7

Table 2 Performance comparison of TiO_2/C-30 with other modified TiO_2

Electrode state	Capacity at low current rate	Capacity at high current rate	Capacity/current rate/cycle number
Nitrogen rich carbon coated TiO_2 nanoparticles[27]	303/0.1C	87/10C	136/5C/500
Graphene-modified TiO_2 hierarchical film[28]	205/0.5C	76/20C	94/5C/3500
N-doped hollow urchin-like anatase TiO_2@C composite[29]	165/1C	111/10C	—
Carbon@mesoporous TiO_2 nanocrystalline@carbon[30]	244/0.1C	115/5C	191/0.2C/200
TiO_2/C-30 (this work)	245/100 mA g^{-1}	133/1500 mA g^{-1}	160/500 mA g^{-1}/1000

intuitive comparison. TiO_2/C-30 exhibits not only the highest specific capacity but also the highest capacity retention at each current density, demonstrating the superior rate capabilities to the other carbon-coated products. The inferior rate performance of TiO_2/C-20 is related to the discontinuous carbon layers, while that of TiO_2/C-40 to the redundant carbon besides the carbon layers. When the current density returned to 0.1 A g^{-1} after the rate performance test, the capacity recovered to similar values to that at the initial 0.1 A g^{-1}, denoting the excellent performance stability of TiO_2/C.

The cells were continued cycling at 0.5 A g^{-1} for exploring the cyclability (Fig. 4c). After 1000 cycles, the capacity is 156.1, 160.0 and 168.2 mA h g^{-1} for TiO_2/C-20, TiO_2/C-30 and TiO_2/C-40, respectively, further confirming the excellent cycling stability after forming the thin carbon layers derived from CA.

The performance of TiO_2/C-30 was also compared with other modified TiO_2 in literature (Table 2). With respect to the highly pure TiO_2 derived from tetraethyl orthotitanate,[27] tetra-*n*-butyl titanate,[28] titanium isopropoxide[29,30] as well as modified by other carbon materials, TiO_2/C-30 reveals the performance comparable to that in the literature despite the simply fabrication of TiO_2/C-30 by employing the cheap raw materials of c-TiO_2 and CA.

3.5. Electrochemical reaction analysis

CV profiles were measured to compare the lithiation/delithiation of TiO_2 and TiO_2/C (Fig. 5). The analogous plots manifest the similar reactions occurred in TiO_2/C to those in TiO_2. The lithiation/delithiation potentials around 1.5/2.4 V associate with the reaction $TiO_2 + xLi^+ + xe^- \leftrightarrow Li_xTiO_2$ ($0 \leq x \leq 1$).[31] The cathodic peak around 0.7 V in the 1st cycle is related to the formation of the SEI films, which disappears in the subsequent cycles. The difference (ΔV) between the anodic (V_a)/cathodic potentials (V_c) for the initial three CV cycles are given in Table 3, which reflects the polarization of the electrode materials to a certain degree. Roughly, the ΔV value for TiO_2 is larger than those for TiO_2/C with the same cycle due to the poor

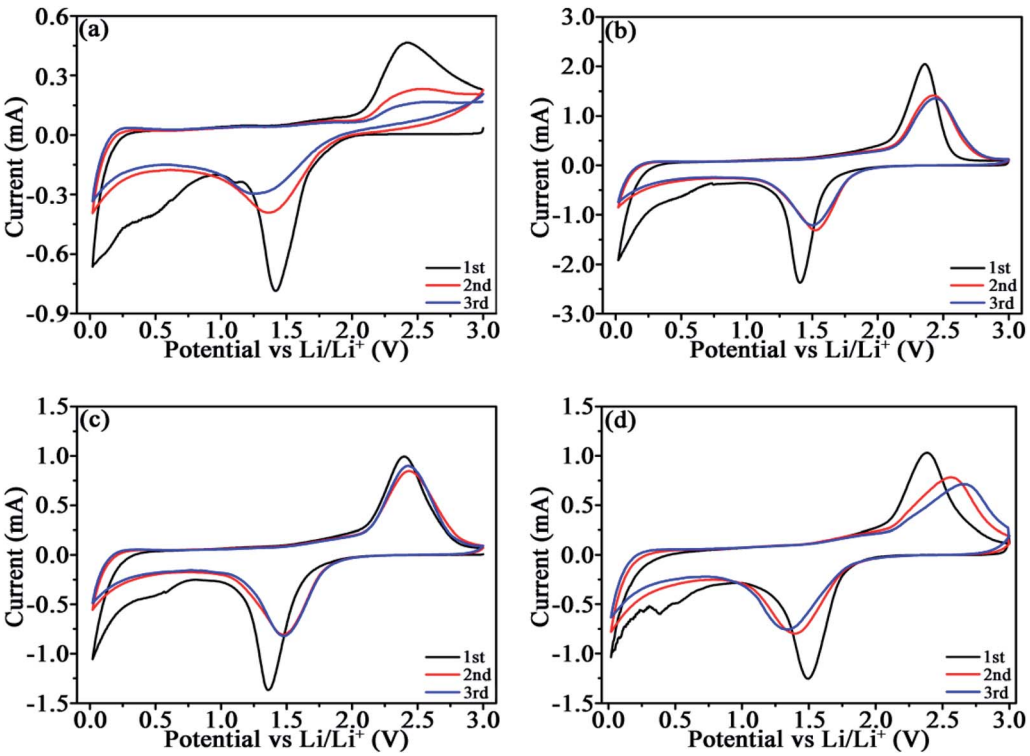

Fig. 5 CV plots of TiO_2 (a), TiO_2/C-20 (b), TiO_2/C-30 (c), and TiO_2/C-40 (d) at 0.3 mV s^{-1}.

Table 3 Difference between the anodic and cathodic potentials for the first three CV cycles

	1st cycle			2nd cycle			3rd cycle		
Samples	V_a	V_c	ΔV	V_a	V_c	ΔV	V_a	V_c	ΔV
TiO_2	2.41	1.42	0.99	2.49	1.37	1.12	2.67	1.28	1.39
TiO_2/C-20	2.37	1.41	0.96	2.43	1.53	0.90	2.44	1.51	0.93
TiO_2/C-30	2.40	1.36	1.04	2.43	1.48	0.95	2.43	1.48	0.95
TiO_2/C-40	2.39	1.49	0.90	2.56	1.40	1.16	2.66	1.35	1.3

electronic conductivity of c-TiO_2. The ΔV for TiO_2/C-20 and TiO_2/C-30 is comparatively stable within the three cycles, while that for TiO_2/C-40 increases with cycling, because carbon materials usually exhibit inferior Li-ion conductivity, meanwhile, the redundant porous carbon results in more SEI films and thus elevated electrical resistance owing to the insulating feature of the SEI films.

3.6. EIS analysis

EIS were measured after cycling the cells for 50 times at 0.1 A g^{-1} to further recognize the effect of carbon on the electrochemical kinetics (Fig. 6). In the equivalent circuit fitting to the EIS (Fig. 6a), R_s stands for the electrolyte resistance, R_{SEI} for the SEI film resistance (acquired by the semicircle diameter in high frequency region[32]), R_{ct} for the charge transfer resistance, CPE for the constant phase elements relevant to interfacial capacitance, and Z_w for the Warburg impedance associating with Li^+ diffusion dynamics. Apparently, the fitting curves almost overlap with the experimental ones (more details at high frequency are displayed in Fig. 6b), corroborating the validity of the equivalent circuit. The data acquired from the fitting plots are collected in Table 4. The total resistance $R_T = (R_s + R_{SEI} + R_{ct})$ for TiO_2/C is significantly smaller than that for TiO_2, demonstrating the markedly enhanced electronic conductivity by coating the thin carbon layers.[33] However, TiO_2/C-40 exhibits higher R_{SEI}, R_{ct}, and R_T than TiO_2/C-30, because the redundant carbon in TiO_2/C-40 gives rise to more SEI films due to the loose porous structure. The SEI film is favorable for Li-ion transfer yet unfavorable for electron migration, resulting in the increased R_{SEI}, R_{ct} and R_T.[34]

Furthermore, Li^+ diffusion coefficient (D) was calculated by the formula $I_p = 2.69 \times 10^5 n^{3/2} A D^{1/2} \nu^{1/2} \Delta C_0$,[35] where I_p – peak current (taking the anodic peak of the stable 3rd CV cycle in Fig. 5 as an example), ΔC_0 – change of Li^+ concentration during discharging/charging (listed in Table 5), $n = 1$ for TiO_2, $A = 1.5386$ cm^2 and $\nu = 3 \times 10^{-4}$ V s^{-1}. From the calculated D values in Table 5, the thin carbon coating brings about the enhancement in ionic conductivity more than one order of magnitude. However, the conductivity decreases slightly with increasing the carbon content due to the poor Li-ion conductivity of carbon materials.

Table 4 Impedance values acquired from fitted EIS plots

Sample	R_s (Ω)	R_{SEI} (Ω)	R_{ct} (Ω)	R_T (Ω)
TiO_2	7.1	500.7	3649.0	4156.8
TiO_2/C-20	5.7	34.5	120.7	160.9
TiO_2/C-30	6.6	50.2	61.8	118.6
TiO_2/C-40	6.3	201.7	299.6	507.6

Table 5 Peak current for the third CV cycle and other parameters for calculating the D value

Samples	I_p (mA)	a (Å)	b (Å)	c (Å)	ΔC_0 (mol cm^{-3})	D (cm^2 S^{-1})
TiO_2	0.17	3.784	3.784	9.515	0.0244	9.45×10^{-13}
TiO_2/C-20	1.35	3.784	3.784	9.515	0.0244	5.96×10^{-11}
TiO_2/C-30	0.90	3.784	3.784	9.515	0.0244	2.65×10^{-11}
TiO_2/C-40	0.71	3.784	3.784	9.515	0.0244	1.64×10^{-11}

Comprehensively considering the electronic and ionic conductivities, the appropriate carbon content to form uniform thin layers (say TiO_2/C-30) is essential for c-TiO_2 to achieve the optimized electrochemical performance.

3.7. Discussion

The performance of the carbon-coated c-TiO_2 was discussed by combining the TEM, EIS, TGA, and CV results in this work with that reported in the literature available,[17,18,36] as summarized in Table 6. Although the interaction with carbon could bring about great improvement in electrochemical performance of c-TiO_2, the performance is still affected by several factors, such as the carbon source, carbonization temperature and resultant carbon content. When c-TiO_2 was calcined at 450 °C with the carbon

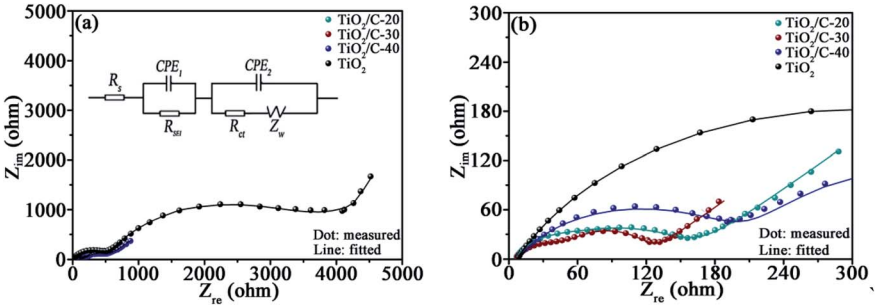

Fig. 6 (a) EIS and the corresponding fitting curves (the inset is the equivalent circuit fitting to the EIS of TiO_2/C), (b) the enlarged EIS at high frequency.

Table 6 Data comparison for TiO_2/C-30 with those in the literature for c-TiO_2-concerned anodes (unit: capacity – mA h g^{-1}, current density – A g^{-1}, capacity retention – %, temperature – °C, CE – %)

Carbon source	Carbonization temperature	Carbon content	Capacity at low rate/ initial CE	Capacity at high rate/ capacity retention	Capacity at 0.5 A g^{-1} after cycling/ cycle number
Sucrose[36]	450	1.9	231 (0.03)	130.0 (0.3)	
Glucose[17]	750	11.7	274.9 (0.1)/47.1	100.7 (1.6)/36.6	203.4/250
Pitch[18]	750	26.6	326.8 (0.1)/46.6	162.5 (1.6)/49.7	140.2/1000
Pitch[37]	900	10.3	180.7 (0.1)/40.5	71.6 (1.6)/39.6	155.8/800
Citric acid	750	2.98	245.8 (0.1)/55.3	133.7 (1.5)/54.4	160.0/1000

precursor of sucrose,[36] the carbon/TiO_2 nanocomposites only revealed better performance at low current rate because of the low carbonization temperature. When the sintering temperature was raised to 750 °C using glucose as the carbon precursor, both the capacity and rate performance were further ameliorated due to the thorough removal of the residual SO_4^{2-} in c-TiO_2. When employing pitch as the carbon source,[18] the products calcined at 750 °C demonstrated high capacity, outstanding rate capabilities and cyclability. However, if the carbonization temperature was raised to 900 °C,[37] the performance decreases despite the amelioration in electronic conductivity by introducing Ti_9O_{17} yet with the reduction in active components. Consequently, compared to the performance of c-TiO_2 in the literature, TiO_2/C-30 demonstrates higher initial CE, superior rate performance and cyclability.

With respect to the carbon precursors of sucrose, glucose and pitch, a protrudent feature of CA lies in the carboxyl groups which could strongly interact with TiO_2 to form self-assembled carboxylate monolayers on the surface of TiO_2.[19] The high-affinity adsorption is conducive to yielding uniform few-layered carbon coating during carbonization, thus not only meliorating the electronic conductivity of TiO_2 but also avoiding the reduction in ionic conductivity caused by the thick carbon layer and redundant carbon. So the few-layered carbon derived from CA is greatly different from the carbon yielded by sucrose, glucose and pitch. The carbon produced by glucose and sucrose usually exhibits porous structure, and the c-TiO_2 particles are more like embedding in the porous carbon instead forming carbon layers on the surface of c-TiO_2 particles. Carbon-coated c-TiO_2 could be obtained using pitch as the carbon precursor, but the content of pitch is frequently high to form the full carbon coating around the c-TiO_2 particles due to the poor interaction between pitch and c-TiO_2, inevitably yielding some redundant loose carbon. As revealed by EIS, the redundant carbon will lead to more SEI films and elevated SEI resistance (Fig. 6), as well as decreased ionic conductivity owing to the inferior Li-ion conductivity of carbon materials (Table 5). As a consequence, the uniform few-layered carbon coating derived from the intense interaction between TiO_2 and CA simultaneous meliorates the electronic and ionic conductivities of c-TiO_2, giving rise to the markedly enhanced performance. This new strategy to achieve uniform and thin carbon coating on the c-TiO_2 particles might be extended to other Ti-containing oxides by employing other carbon sources with carboxyl groups for optimizing the comprehensive electrochemical performance.

4. Conclusions

In summary, uniform thin carbon coating about 2–3 carbon layers in thickness could be easily formed on the c-TiO_2 particles by adopting CA as the carbon source followed by carbonizing the mixture at 750 °C. Herein the high-affinity adsorption of TiO_2 for carboxyl groups to form self-assembled carboxylate monolayers on the surface of TiO_2 is conducive to yielding the uniform and thin carbon layers during carbonization which could further endow the c-TiO_2 with the enhanced electronic and ionic conductivities, attenuated polarization, and thus the elevated capacity and excellent long-term cycling stability. The strategy might be extended to other Ti-containing oxides by employing other carbon sources with carboxyl groups for achieving uniform few-layered carbon coating to optimize the performance. Moreover, the simply processing with environmental benignity as well as the low cost carbon source of CA allows the carbon coating strategy applicable in industrial production of c-TiO_2 anodes for LIBs.

Conflicts of interest

There are no conflicts to declare.

Acknowledgements

This work was supported by project ZR2019MEM029 of Natural Science Foundation of Shandong Province, PR China.

References

1 W. Wen, J.-M. Wu, Y.-Z. Jiang, S.-L. Yu, J.-Q. Bai, M.-H. Cao and J. Cui, *Sci. Rep.*, 2015, **5**, 11804.
2 G.-N. Zhu, Y.-G. Wang and Y.-Y. Xia, *Energy Environ. Sci.*, 2012, **5**, 6652–6667.
3 J. Zhang, X. Yan, J. Zhang, W. Cai, Z. Wu and Z. Zhang, *J. Power Sources*, 2012, **198**, 223–228.
4 Z. Chen, I. Belharouak, Y. K. Sun and K. Amine, *Adv. Funct. Mater.*, 2013, **23**, 959–969.
5 Y.-M. Jiang, K.-X. Wang, X.-X. Guo, X. Wei, J.-F. Wang and J.-S. Chen, *J. Power Sources*, 2012, **214**, 298–302.
6 M. Wagemaker, G. J. Kearley, A. A. van Well, H. Mutka and F. M. Mulder, *J. Am. Chem. Soc.*, 2003, **125**, 840–848.
7 Z. Ali, S. N. Cha, J. I. Sohn, I. Shakir, C. Yan, J. M. Kim and D. J. Kang, *J. Mater. Chem.*, 2012, **22**, 17625–17629.

8 T. Song, H. Han, H. Choi, J. W. Lee, H. Park, S. Lee, W. I. Park, S. Kim, L. Liu and U. Paik, *Nano Res.*, 2015, **7**, 491–501.
9 X. Chen and S.-S. Mao, *Chem. Rev.*, 2007, **107**, 2891–2959.
10 W. Li, F. Wang, Y. Liu, J. Wang, J. Yang, L. Zhang, A. A. Elzatahry, D. M. Aldhayan, Y. Xia and D. Zhao, *Nano Lett.*, 2015, **15**, 2186–2193.
11 L. Zhao, S. Wang, F. Pan, Z. Tang, Z. Zhang, S. Zhong and J. Zhang, *J. Mater. Chem. A*, 2018, **6**, 11688–11693.
12 G. D. Park, J. H. Hong, J. K. Lee and Y. C. Kang, *Nanoscale*, 2019, **11**, 631–638.
13 C. Wang, L. Wu, H. Wang, W. Zuo, Y. Li and J. Liu, *Adv. Funct. Mater.*, 2015, **25**, 3524–3533.
14 J.-Y. Liao, D. Higgins, G. Lui, V. Chabot, X. Xiao and Z. Chen, *Nano Lett.*, 2013, **13**, 5467–5473.
15 Y. Wu, C. Zhu, L. Shu, J. Duan, D. Wei, J. Xu, Z. Zhu, L. Li, Z. Peng and Z. Chen, *Appl. Surf. Sci.*, 2019, **489**, 528–537.
16 C. Zhao, L. Liu, Q. Zhang, J. Rogers, H. Zhao and Y. Li, *Electrochim. Acta*, 2015, **155**, 288–296.
17 L.-Y. Wang, Y. Wu, J.-P. Han, B. Zhang, X. Bai, Y.-X. Qi, N. Lun, Y.-M. Cao and Y.-J. Bai, *Electrochim. Acta*, 2017, **245**, 186–192.
18 L.-Y. Wang, X. Bai, Y. Wu, N. Lun, Y.-X. Qi and Y.-J. Bai, *Electrochim. Acta*, 2016, **212**, 155–161.
19 J. Balajka, M. A. Hines, D. B. Wji, M. Komora, J. Pavelec, M. Schmid and U. Diebold, *Science*, 2018, **361**, 786–789.
20 N. Venkatachalam, M. Palanichamy and V. Murugesan, *J. Mol. Catal. A: Chem.*, 2007, **273**, 177–185.
21 B. Naik, K. M. Parida and C. S. Gopinath, *J. Phys. Chem. C*, 2010, **114**, 19473–19482.
22 G. Trettenhahn and A. Köberl, *Electrochim. Acta*, 2007, **52**, 2716–2722.
23 K. Umemura, T. Ueda, S. S. Munawar and S. Kawai, *J. Appl. Polym. Sci.*, 2011, **123**, 1991–1996.
24 V. Swamy, A. Kuznetsov, L. S. Dubrovinsky, R. A. Caruso, D. G. Shchukin and B. C. Muddle, *Phys. Rev. B: Condens. Matter Mater. Phys.*, 2005, **71**, 184302.
25 W. Zhang, Y. He, M. Zhang, Z. Yin and Q. Chen, *J. Phys. D: Appl. Phys.*, 2000, **33**, 912–916.
26 T. Zhao, D. Zhu, W. Li, A. Li and J. Zhang, *J. Power Sources*, 2019, **439**, 227027.
27 C. Senthil, T. Kesavan, A. Bhaumik, M. Yoshio and M. Sasidharan, *Electrochim. Acta*, 2017, **255**, 417–427.
28 H. Luo, C. Xu, B. Wang, F. Jin, L. Wang, T. Liu, Y. Zhou and D. Wang, *Electrochim. Acta*, 2019, **313**, 10–19.
29 Y. Xing, S. Wang, B. Fang, G. Song, D. P. Wilkinson and S. Zhang, *J. Power Sources*, 2018, **385**, 10–17.
30 W. Yan, Y. Yuan, J. Xiang, Y. Wu, T. Zhang, S. Yin and S. Guo, *Electrochim. Acta*, 2019, **312**, 119–127.
31 G. Nuspl, K. Yoshizawa and T. Yamabe, *J. Mater. Chem.*, 1997, **7**, 2529–2536.
32 M. S. Kim, B. Fang, J. H. Kim, D. Yang, K. K. Yun, T. S. Bae and J. S. Yu, *J. Mater. Chem.*, 2011, **21**, 19362–19367.
33 D. Wang, D. Choi, J. Li, Z. Yang, Z. Nie, R. Kou, D. Hu, C. Wang, L. V. Saraf and J. Zhang, *ACS Nano*, 2009, **3**, 907–914.
34 J. Wang, X.-M. Liu, H. Yang and X.-D. Shen, *J. Alloys Compd.*, 2011, **509**, 712–718.
35 A. J. Brad and L. R. Faulkner, *Electrochemical methods: fundamentals and applications*, vol. 2, Wiley-VCH, New York, 1980.
36 C. Zhao, L. Liu, Q. Zhang, J. Rogers, H. Zhao and Y. Li, *Electrochim. Acta*, 2015, **155**, 288–296.
37 J.-X. Teng, R.-L. Bai, L.-Y. Wang and Y.-J. Bai, *J. Alloys Compd.*, 2018, **762**, 594–604.